Received: 22 December 2021 | Revised: 5 May 2022 | Accepted: 5 May 2022

DOI: 10.1111/apha.13828

ACTA PHYSIOLOGICA

RENAL PHYSIOLOGY

Increased COX-2 after ureter obstruction attenuates fibrosis and is associated with EP_2 receptor upregulation in mouse and human kidney

Signe S. Tofteng[1] | **Line Nilsson**[2] | **Amalie K. Mogensen**[1] | **Rikke Nørregaard**[2] | **Rolf Nüsing**[3] | **Mikhail Diatchikhine**[4] | **Lars Lund**[4,5] | **Claus Bistrup**[5,6] | **Boye L. Jensen**[1] | **Kirsten Madsen**[1,7]

[1]Department of Cardiovascular and Renal Research, Institute of Molecular Medicine, University of Southern Denmark, Odense, Denmark

[2]Department of Clinical Medicine, Aarhus University, Aarhus, Denmark

[3]Institute of Clinical Pharmacology, Goethe University, Frankfurt, Germany

[4]Department of Urology, Odense University Hospital, Odense, Denmark

[5]Department of Clinical Research, University of Southern Denmark, Odense, Denmark

[6]Department of Nephrology, Odense University Hospital, Odense, Denmark

[7]Department of Pathology, Odense University Hospital, Odense, Denmark

Correspondence
Kirsten Madsen, Department of Cardiovascular and Renal Research, Institute of Molecular Medicine, University of Southern Denmark, J. B. Winsloews Vej 21,3, DK-5000 Odense C, Denmark.
Email: kmadsen@health.sdu.dk

Funding information
Aarhus University Research Foundation, Grant/Award Number: AUFF-E-2015-FLS-8-69; Aase og Ejnar Danielsens Foundation; Danish Society of Nephrology; Danish Counsil for Independent Research, Grant/Award Number: 6110-00231B; Familien Hede Nielsens Foundation; Helen og Ejnar Bjørnows Foundation; Danish Kidney Association; Odense University Hospital PhD Fund, University of Southern Denmark; The A. P. Møller Foundation for the Advancement of Medical Science

Abstract

Aim: Cyclooxygenase-2 (COX-2) activity protects against oxidative stress and apoptosis early in experimental kidney injury. The present study was designed to test the hypothesis that COX-2 activity attenuates fibrosis and preserves microvasculature in injured kidney. The murine unilateral ureteral-obstruction (UUO) model of kidney fibrosis was employed and compared with human nephrectomy tissue with and without chronic hydronephrosis.

Methods: Fibrosis and angiogenic markers were quantified in kidney tissue from wild-type and COX-$2^{-/-}$ mice subjected to UUO for 7 days and in human kidney tissue. COX-enzymes, prostaglandin (PG) synthases, PG receptors, PGE_2, and thromboxane were determined in human tissue.

Results: COX-2 immunosignal was observed in interstitial fibroblasts at baseline and after UUO. Fibronectin, collagen I, III, alpha-smooth muscle actin, and fibroblast specific protein-1 mRNAs increased significantly more after UUO in COX-$2^{-/-}$ vs wild-type mice. In vitro, fibroblasts from COX-$2^{-/-}$ kidneys showed higher matrix synthesis. Compared to control, human hydronephrotic kidneys showed (i) fibrosis, (ii) no significant changes in COX-2, COX-1, PGE_2-, and prostacyclin synthases, and prostacyclin and thromboxane receptor mRNAs, (iii) increased mRNA and protein of PGE_2-EP_2 receptor level but unchanged PGE_2 tissue concentration, and (iv) two- to threefold increased thromboxane synthase

mRNA and protein levels, and increased thromboxane B_2 tissue concentration in cortex and outer medulla.

Conclusion: COX-2 protects in the early phase against obstruction-induced fibrosis and maintains angiogenic factors. Increased PGE_2-EP_2 receptor in obstructed human and murine kidneys could contribute to protection.

KEYWORDS

angiogenesis, hydronephrosis, obstruction, prostaglandin E_2, thromboxane

1 | INTRODUCTION

Tubulointerstitial fibrosis is the final common endpoint for most chronic kidney diseases (CKD) and is characterized by an interstitial expansion through accumulation of extracellular matrix (ECM) proteins, tubular atrophy, and loss of peritubular capillaries. This leads to nephron regression, impaired glomerular filtration rate, chronic ischemia, and loss of kidney function.[1–4] Locally, at the tissue level, prostaglandin E_2 (PGE_2), thromboxane, and prostacyclin may play a significant role in fibrosis progression. Cyclooxygenase-2 (COX-2) is increased in response to kidney injury.[5,6] Acutely, COX-2 is upregulated mainly in the inner medulla in rodent models of ureter obstruction.[7,8] Here, it transiently contributes to the accumulation of PGE_2[9] but also thromboxane (Tx) B_2, 6-keto-$PGF_{1\alpha}$, and $PGF_{2\alpha}$ in rats.[10] The acute ureter obstruction-induced COX-2 activity promotes downregulation of aquaporins (AQPs) and NaCl transporters[7,11–13] and protects against oxidative stress, tubular injury, and apoptosis.[14] The accumulated data suggest a protective role for COX-2-derived PGE_2—at least in the early stages of injury. The significance of the COX-2 pathway for progression to kidney fibrosis at the more chronic stage is less clear. Here, the observed parallel stimulation of TxA_2 and $PGF_{2\alpha}$ in obstruction could have opposite effects on PGE_2.[10] Moreover, COX-2 activity may lead to the formation of different prostanoids in resident versus invading cells, like macrophages[15,16] that could contribute differentially to the integrated, long-term, response of fibrosis. Rodent models of renal ablation[15,17] puromycin amino nucleoside-induced kidney injury,[18] and in siRNA induced COX-2 knockdown in macrophages suggests a pathogenic role of COX-2.[19] Thus, COX-2 is pleiotropic. There is an overweight of data on COX-2 PGE_2 signaling in rodent models and less knowledge on this pathway in the human kidney. Use of nonsteroidal anti-inflammatory drugs (NSAIDs) is associated with increased risk of CKD progression in patients with hypertension[20] and in elderly (aged ≥66 years) exposed to a high cumulative NSAID dosage.[21] In vitro and in vivo studies have shown anti-fibrotic effects of PGE_2 in lung,[22–28] liver/hepatocytes,[29,30] and the intestine through the activation of EP_2 and EP_4 receptors.[31] We showed previously a significant upregulation of PGE_2 receptors EP_1 but particularly EP_2 and EP_4 after 7 days of UUO in mice.[14] Using pharmacological tools and EP knockout (KO) models, subsequent studies showed beneficial effects of PGE_2 in the progression of renal fibrosis,[32,33] accounted for by the microsomal prostaglandin synthase-1 (mPGES-1)/PGE_2/EP_4 pathway.[34] The present study was designed to investigate the role of COX-2 in development and progression of renal fibrosis after 7 days UUO in wild-type and COX-2 KO mice. The aim was to compare findings with the closest human correlate: nephrectomy tissue from patients with histo-pathologically confirmed chronic ureter obstruction at the time of nephrectomy. Specifically, experiments were designed to test the hypotheses that (1) COX-2 protects against the development of kidney fibrosis, through (2) PGE_2-mediated attenuation of renal fibroblast activity and production of extracellular matrix, and (3) through consistency of capillaries by supporting angiogenic factors. Human kidneys with chronic hydronephrotic changes were predicted to display similar changes compared with control kidneys without hydronephrosis. Tissue was analyzed by combined qPCR, western blotting, ELISA, immunohistochemistry, and mass spectrometry.

2 | RESULTS

2.1 | Basic characteristics and plasma parameters

The four experimental groups in Table 1 (WT Sham, COX-2 KO Sham, WT 7dUUO, and COX-2 KO 7dUUO) showed no difference in body weight. At baseline, COX-2 deficient mice showed lowered obstructed kidney weight by 30% compared to wild-type littermate controls. Wild-type and COX-2 KO obstructed kidney weight was 35% and 40% higher after UUO compared to sham-operated mice, respectively. The kidney weight of COX-2 deficient UUO vs. wild-type mice was 25% lower. Similar results

TABLE 1 Basic characteristics and plasma data for the four experimental groups of mice

	WT Sham	COX-2 KO Sham	WT 7dUUO	COX-2 KO 7dUUO
Gender ratio (male:female)	10:7	6:6	9:8	7:4
Body weight (g)	27.1 ± 1.0 ($n = 17$)	25.8 ± 1.2 ($n = 12$)	25.6 ± 1.1 ($n = 17$)	25.2 ± 1.3 ($n = 11$)
Obstructed kidney weight (mg g^{-1} BW)	6.4 ± 0.1 ($n = 17$)	4.9 ± 0.2* ($n = 12$)	8.7 ± 0.3§ ($n = 17$)	6.9 ± 0.3$^{\Phi,\forall}$ ($n = 11$)
Contralateral kidney weight (mg g^{-1} BW)	6.4 ± 0.1 ($n = 17$)	5.0 ± 0.1* ($n = 12$)	7.5 ± 0.1§ ($n = 17$)	6.1 ± 0.2$^{\Phi,\forall}$ ($n = 11$)
Plasma Osmolality (mOsmol kg^{-1} H_2O)	310.8 ± 4.8 ($n = 16$)	321.9 ± 5.0 ($n = 9$)	313.1 ± 2.6 ($n = 14$)	320.8 ± 5.0 ($n = 11$)
Plasma Na^+ (mmol L^{-1})	146.9 ± 0.4 ($n = 10$)	146.1 ± 0.4 ($n = 7$)	147.6 ± 0.5 ($n = 8$)	147.0 ± 0.4 ($n = 9$)
Plasma K^+ (mmol L^{-1})	4.1 ± 0.1 ($n = 10$)	4.1 ± 0.1 ($n = 7$)	3.9 ± 0.2 ($n = 8$)	4.4 ± 0.1 ($n = 9$)
Plasma Creatinine (μmol L^{-1})	8.5 ± 0.1 ($n = 11$)	10.3 ± 1.8 ($n = 6$)	10.1 ± 0.01 ($n = 14$)	15.3 ± 1.8$^{\forall}$ ($n = 6$)
Urea (mmol L^{-1})	8.30 ± 0.7 ($n = 11$)	20.5 ± 1.9* ($n = 7$)	10.5 ± 0.5 ($n = 9$)	25.9 ± 1.5$^{\Phi,\forall}$ ($n = 9$)

Note: Effect of COX-2 knockout and unilateral ureteral obstructions on whole body and kidney weight and plasma parameters. Values are presented as mean ± SEM, and marked with a symbol, when statistically significant ($p < 0.05$); WT sham vs. COX-2 KO sham (*) WT sham vs. WT UUO (§), COX-2 KO sham vs. COX-2 KO UUO ($^{\Phi}$), and WT UUO vs. COX-2 KO UUO ($^{\forall}$).

were obtained for contralateral kidney weight that was 30% lower in COX-2 deficient mice compared to wild-type littermates and higher by 20% after obstruction for both genotypes. Contralateral kidney weight for COX-2 deficient UUO mice vs. wild-type littermates also was 20% lower.

Plasma osmolality, sodium, and potassium concentrations did not differ between groups (Table 1). At baseline, plasma creatinine was not different between genotypes but was significantly higher in COX-2 KO mice after UUO compared to wild-type littermate controls (15.3 ± 1.8 vs. 10.1 ± 0.01, units μmol L^{-1}). Mice with COX-2 deficiency displayed significantly increased plasma urea concentrations at baseline (20.5 ± 1.9 vs. 8.3 ± 0.7, units mmol L^{-1}). COX-2 KO mice had a significantly increased plasma urea level after UUO compared to sham-operated controls (25.9 ± 1.5 vs. 10.5 ± 0.5, units mmol L^{-1}).

2.2 | Kidney fibrosis markers in COX-2 deficient mice and wild-type littermate controls in response to unilateral ureteral obstruction

No significant interstitial fibrosis was detected in sham-operated COX-2 KO mice and in wild-type littermate controls (Figure 1A,E). Kidneys from COX-2 KO mice subjected to sham surgery showed a slightly reduced cortical thickness compared to wild-type littermates (Figure 1A,E) and an increased number of small glomeruli in the subcapsular region not seen in wild-types (data not shown). After 7 days UUO, significant kidney tissue injury was seen with expansion of the pelvic space, papillary atrophy, reduced cortical, and outer medullary thickness, tubular damage, and extracellular matrix (ECM) accumulation in the interstitium (Figure 1A–H). The renal outer medulla was the most severely affected region in both genotypes (Figure 1D,H). Tubular damage and interstitial ECM accumulation were more severe in COX-2 KO mice compared to wild-type controls (Figure 1B–D,F–H). Kidney tissue collagen I, collagen III, and fibronectin mRNA abundances did not show significant differences between sham-operated COX-2 KO mice and wild-type control animals (Figure 1I–K). However, mRNA levels of both collagen I, collagen III, and fibronectin increased 20- to 30-fold after 7 days UUO in both COX-2 KO and wild-type mice compared to sham groups of both genotypes (Figure 1I–K). Moreover, mRNA abundance of all three ECM components increased to a significantly higher level in obstructed COX-2 KO mice compared to wild-type controls (Figure 1I–K). Total collagen accumulation as analyzed by hydroxyproline assessment in whole kidney tissue from wild-type and COX-2 KO mice was not significantly different between sham and UUO tissue and genotypes (Figure 1L). Immunohistochemical labeling for collagen I in kidney tissue sections from all four experimental groups showed an interstitial signal for collagen I in both COX-2 KO and wild-type mice after 7 days UUO

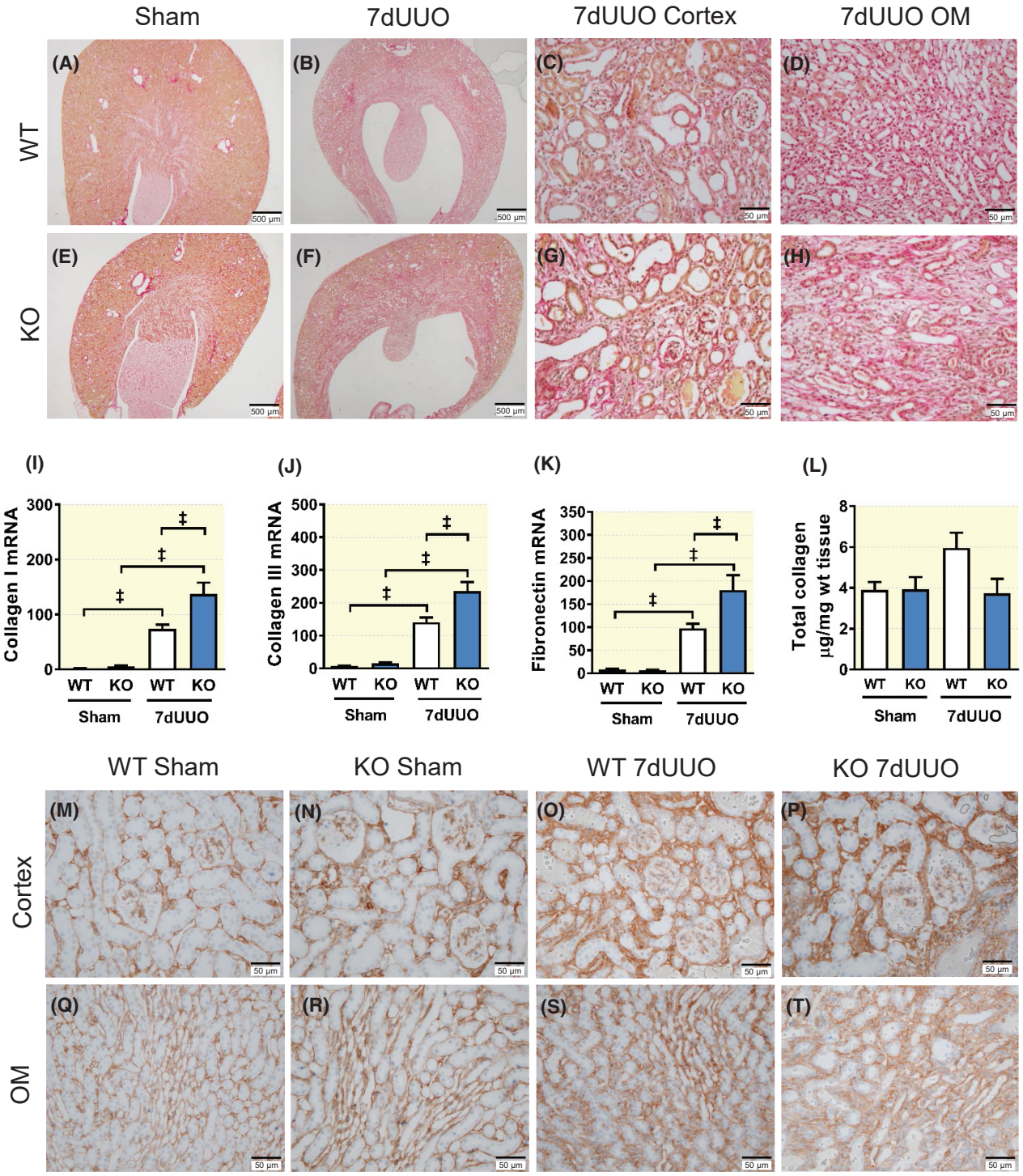

FIGURE 1 Kidney fibrosis in COX-2 deficient mice and wild-type littermate controls in response to 7 days of unilateral ureter obstruction (UUO). Kidney tissue sections from mice with and without UUO and COX-2 were stained with Sirius Red to visualize collagen/connective tissue in red (A, B, E, and F scale bar 500 µm and C, D, G, and H scale bar 50 µm). COX-2 deficiency (COX-2 KO) lead to a slight reduction in cortical thickness (A and E) but no difference in kidney injury after 7dUUO compared to wild-type (C, D, G, and H). Diagram (I–K) show cortex-outer medulla tissue abundance of extracellular matrix proteins collagen I (I), collagen III (J), and fibronectin (K) mRNAs in COX-2 deficient mice (KO) and wild-type littermate controls (WT) after sham and 7dUUO. Diagram (L) shows total collagen level in kidney tissue from all four experimental groups. (WT sham: $n = 17$, COX-2 KO sham: $n = 12$, WT 7dUUO: $n = 17$, and COX-2 KO 7dUUO: $n = 11$) (‡) $p < 0.001$. Micrographs m-t show result of immunohistochemical labeling for collagen I in kidney sections from COX-2 deficient mice (KO) and wild-type littermate controls (WT) after sham surgery and ureter obstruction (7dUUO; M–T) (WT sham: $n = 5$, COX-2 KO sham: $n = 3$, WT 7dUUO: $n = 4$, and COX-2 KO 7dUUO: $n = 3$).

with the outer medulla being the region most severely affected in both genotypes (Figure 1O,P,S,T). No significant accumulation of collagen I was seen in COX-2 KO sham mice compared to wild-type controls (Figure 1M,N,Q,R). Also, deletion of COX-2 did not significantly increase interstitial collagen I protein deposition after obstruction compared to wild-type littermates in cortex or outer medulla regions (Figure 1O,P,S,T). An identical pattern of collagen III interstitial accumulation of immunosignal was seen in all four experimental groups (Figure S1A–L). Stereological unbiased assessment of the collagen I-positive area in COX-2 KO and wild-type sham and UUO mice ($n = 3$ in each group) showed a mean of 19% (±1.6) interstitial collagen I in wild-type sham mice, 21% (±2) in COX-2 KO sham mice, 47% (±2.8) in wild-type UUO mice, and 51% (±1.2) in COX-2 KO UUO mice.

2.3 | Renal fibroblast abundance in COX-2 deficient mice and wild-type littermate controls in response to unilateral ureteral obstruction

Quantitative determination of markers of renal fibroblasts showed no significant difference in α-SMA or fibroblast specific protein-1 (FSP-1) mRNA abundance between genotypes in the two sham-operated groups (Figure 2A,C). Both α-SMA and FSP-1 mRNA abundance increased significantly in response to 7 days UUO in COX-2 KO mice and wild-type control animals (Figure 2A,C). The increase in α-SMA mRNA was significantly larger in COX-2 KO mice compared to the wild-type group (Figure 2A). Changes in α-SMA were confirmed at the protein level with increased α-SMA protein abundance after 7 days UUO in wild-type animals compared to the sham group (Figure 2B, non-cropped versions in supplement). A tendency for a similar increase was seen in COX-2 KO mice but this did not reach statistical significance (Figure 2B). Immunohistochemical labeling of kidney sections for α-SMA showed a signal confined to smooth muscle cells in the renal vascular walls in both sham-operated wild-type control animals (Figure 2D–E) and COX-2 KO mice (data not shown). After 7 days UUO, accumulation of α-SMA positive cells and interstitial α-SMA was seen in the renal interstitium of both cortex and outer medulla with the outer medulla being the most severely affected region (Figure 2F–I). COX-2 KO mice were not more extensively affected than wild-type mice (Figure 2F–I). Double immunofluorescence staining showed co-expression of COX-2 and α-SMA in cells accumulated in the renal interstitium after 7 days UUO (Figure 2J–N). Fibroblasts grown in primary culture from COX-2 KO mice showed a significantly higher mRNA abundance of collagen I, collagen III, and α-SMA compared to wild-type cells (Figure 2O). Treatment of wild-type fibroblasts with either the non-specific COX inhibitor indomethacin, the COX-2 inhibitor NS-398, or the COX-1 inhibitor valeryl salicylate for 24 h did not induce significant changes in collagen I, collagen III, or α-SMA mRNA abundance (Figure 2P).

2.4 | Renal microvascular integrity and expression of vascular growth factors in COX-2 deficient mice and wild-type littermate controls in response to unilateral ureteral obstruction

Immunohistochemical visualization of the renal microvasculature with an antibody directed against CD34 showed a dense capillary network in the sham-operated groups (Figure 3A,B,E,F). The distribution of micro-vessels was not significantly different between genotypes in both cortex and medulla (Figure 3A,B,E,F). After 7 days UUO, capillary rarefaction with loss of both cortical and outer medullary micro-vessels was evident with no obvious significant difference between genotypes (Figure 3C,D,G,H). Renal mRNA abundance of the vascular growth factors VEGF and angiopoietin-1 was significantly lower in sham-operated COX-2 KO mice compared to control animals (Figure 3I,K). In wild-type mice, the level of VEGF and angiopoietin-1 mRNA was significantly reduced after 7 days UUO reaching the level seen in COX-2 KO mice (Figure 3I,K). No significant changes in mRNA abundance were seen for angiopoietin-2 (Figure 3L). VEGF protein abundance was significantly increased in wild-type obstructed mice compared to the sham control (Figure 3J). In obstructed COX-2 KO mice there was no significant difference in VEGF protein abundance (Figure 3J).

2.5 | Basic characteristics of patients diagnosed with hydronephrosis and control subjects

A total of 12 nephrectomy samples from patients with a histopathological diagnosis of hydronephrosis were included in the study. Kidney tissue from patients undergoing nephrectomy due to kidney cancer but with no clinical or histopathological diagnosis of hydronephrosis were used as controls. Age and gender distributions at the time of nephrectomy, blood pressure, eGFR, plasma urea, and creatinine levels are listed in Table 2. The hydronephrosis group showed significantly higher levels of urea and creatinine, and a significantly lower eGFR compared to controls. The blood pressure was not different between the two groups. A

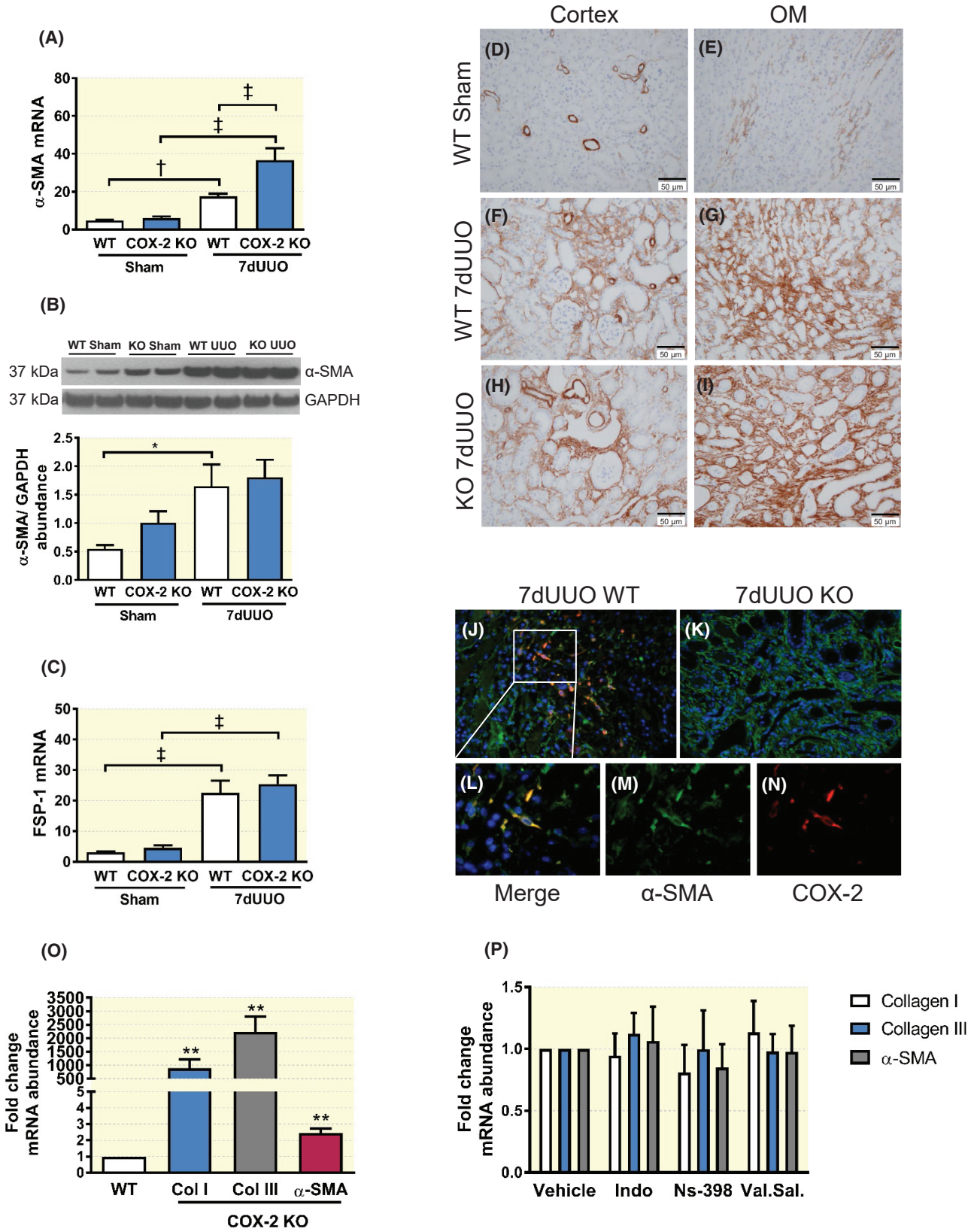

full list of medication and co-morbidity is available in supplements showing more co-morbidities and use of different drugs in the hydronephrosis group vs. control group. The most common co-morbidity in both groups is cancer, and the most apparent difference in medication is the use of analgesics, cancer medication, and blood pressure-lowering medication in the hydronephrosis group. Three patients in the hydronephrosis group vs.

FIGURE 2 Myofibroblast infiltration and collagen accumulation in murine kidneys and cultured fibroblasts. Kidney abundance of myofibroblast marker α-SMA mRNA (A) (WT sham: $n = 17$, COX-2 KO sham: $n = 12$, WT 7dUUO: $n = 17$, and COX-2 KO 7dUUO: $n = 11$) and protein (B, 42 kDa) ($n = 6$ in each group) and FSP-1 mRNA (C) in COX-2 deficient mice (COX-2 KO) and wild-type (WT) littermate controls after sham surgery and 7dUUO. Micrographs in D–I show immunohistochemical labeling experiments of kidney sections for α-SMA. There was accumulation of myofibroblasts in interstitium of cortex and outer medulla (OM) after 7dUUO (G, I) (WT sham: $n = 5$, COX-2 KO sham: $n = 3$, WT 7dUUO: $n = 4$, and COX-2 KO 7dUUO: $n = 3$). Panels J–N show result of double-immunofluorescence labeling for α-SMA (green signal) and COX-2 (red signal) from wild-type and COX-2 deficient mice after 7dUUO (J–N). Interstitial fibroblasts were co-labeled (J) and magnified (L). Diagram (O) shows mRNA abundance of αSMA, collagen I, and collagen III in primary cultures of kidney fibroblasts from COX-2 KO and wild-type mice, and from wild-type mice treated with non-specific COX inhibitor indomethacin, the COX-2 inhibitor Ns-398, or the COX-1 inhibitor valeryl salicylate for 24 h (P). (*) $p < 0.05$, (†) $p < 0.01$, (‡) $p < 0.001$.

one patient in the control group use NSAID/aspirin. Kidney morphology was evaluated in PAS-stained tissue sections. In control subjects, tissue appeared normal with minimal interstitial fibrosis affecting less than 10% of the cortical area (score 0). In the hydronephrosis group, a varying degree of chronic changes were seen with none or minimal interstitial fibrosis in three patients (score 0), mild interstitial fibrosis in four patients (score 1), and moderate to severe interstitial fibrosis in three and two patients (score 2 and 3), respectively (Figure 4A–D). Collagen-1 mRNA abundance was sixfold increased in kidney tissue in the hydronephrosis group (Figure 4E), and α-SMA protein abundance in kidney cortex tissue from patients with hydronephrosis was not significantly different compared to control subjects ($p = 0.0834$, Figure 4F). There was no significant difference in mRNA abundance of COX-2, COX-1, and PTGES mRNA in kidney cortex and outer medulla between patients with overt hydronephrosis/fibrosis and patients with no hydronephrosis (Figure 4G–I).

2.6 | Changes in prostaglandin signaling pathways in patients diagnosed with hydronephrosis

In kidney cortex, PGE_2-EP_2 receptor mRNA abundance was elevated while EP_3 receptor mRNA was lower in kidneys from patient with hydronephrosis compared to control kidneys (Figure 5A). Likewise, PGE_2-EP_3 receptor mRNA abundance was significantly reduced in outer medulla compared to control (Figure 5B). No significant changes in cortical and outer medulla PTGES, EP_1, or EP_4 receptor mRNA abundance were detected (Figure 5A,B). There was no difference in EP receptors or PTGES mRNA abundances in the inner medulla compared to control (Figure 5D). Since EP_2 receptor mRNA level was significantly increased in cortex from the hydronephrosis group, EP_2 receptor protein abundance was also assessed by western blotting in that region (Figure 5D). The EP_2 receptor protein abundance was significantly increased in the hydronephrosis group compared to control and supported EP_2 receptor mRNA data (Figure 5C).

Immunohistochemical detection of EP_2 protein showed significant association with the tubular epithelium in cortex and outer medulla (Figure S2A–F). The immunosignal was predominantly associated with the basolateral domain of the epithelium. In the absence of primary antibody, secondary antibody yielded no signal, and the labeling signal with primary antibody was abolished by pre-incubating the antibody with surplus of immunizing peptide used to raise the antibody (Figure S2). Fluorescently labeled segments for EP_2 (Figure 5E–T) showed co-localization with aquaporin (AQP) -2 but not AQP1 in cortex (Figure 5M–P,E–H) and outer medulla tissue from patients with hydronephrosis (Figure 5Q–T,I–L). Thus, EP_2 immuno-fluorescence signal was found in collecting duct principal cells and not in proximal tubules. EP_2 signal was also present in AQP2- and AQP1-negative tubules which likely represent segments of Henle's Loop. Fluorescently labeled tissue sections for EP_2, AQP1, and AQP2 from control subjects are shown in Figure S2G–N,O–V.

In kidney cortex, outer and inner medulla tissue from patients with hydronephrosis, there was no difference in mRNA level of prostacyclin receptor IP, thromboxane prostanoid receptor TP, and prostacyclin synthase (PGIS) compared to tissue from patients without hydronephrosis (Figure 6A–C). By contrast, thromboxane synthase (TxAS) was significantly increased in outer and inner medulla (Figure 6B,C). TxAS mRNA abundance in cortex was not significantly different (Figure 6A). TxAS-1 protein abundance was significantly higher in cortex and outer medulla tissue from patients with hydronephrosis compared to patients without hydronephrosis (Figure 6D,E). There was no change in TxAS-1 protein level in inner medulla (Figure 6F).

2.7 | Prostanoid abundance in kidney regions from hydronephrotic patients and controls

TxB_2 concentration was increased significantly in kidney cortex tissue from patients with hydronephrosis compared to control subjects (Figure 6G), whereas outer

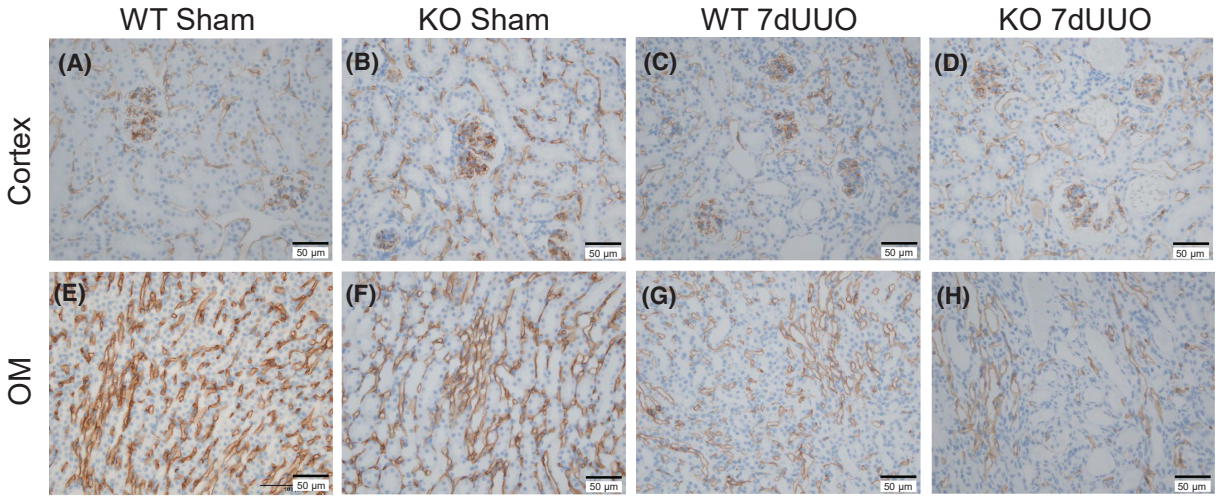

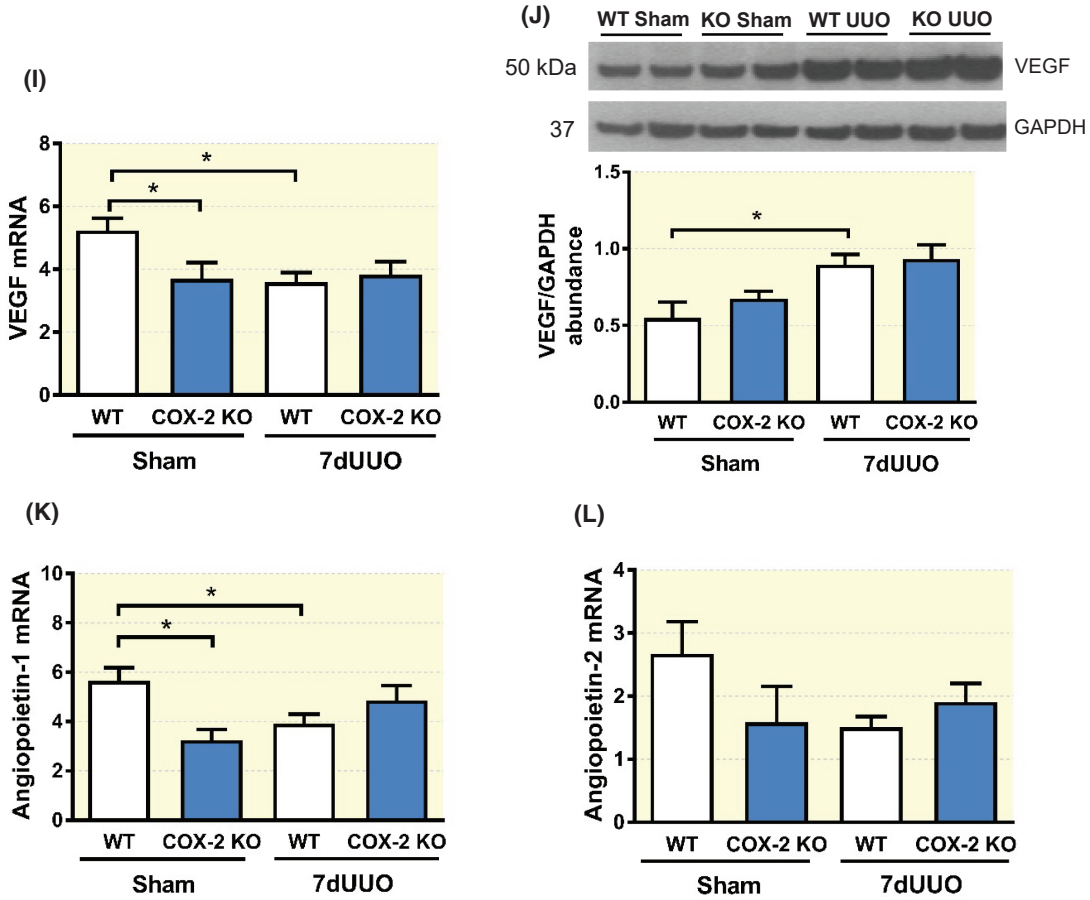

FIGURE 3 Microvascular rarefaction in COX-2 deficient mice and wild-type littermate controls after 7 days of unilateral ureter obstruction (UUO). (A–H) show results from immunohistochemical labeling of kidney sections for the capillary marker CD34 in cortex and outer medulla (OM) from COX-2 deficient mice (COX-2 KO) and wild-type (WT) littermate controls after sham and 7dUUO (WT sham: $n = 5$, COX-2 KO sham: $n = 3$, WT 7dUUO: $n = 4$, and COX-2 KO 7dUUO: $n = 3$). Omission of primary antibody was used as negative control (data not shown). (I–J) show kidney tissue abundance of VEGF mRNA (WT sham: $n = 17$, COX-2 KO sham: $n = 12$, WT 7dUUO: $n = 17$, and COX-2 KO 7dUUO: $n = 11$) and protein (46 kDa) ($n = 6$ in each group) in cortex-outer medulla from COX-2 KO and WT controls, respectively. Diagram (K–L) show kidney cortex-outer medulla tissue abundance of angiopoietin-1 (K) and – 2 (L) in COX-2 KO mice and WT littermate controls. (*) $p < 0.05$.

TABLE 2 Basic characteristics and clinical parameters from patients and control subjects

	Control	Hydronephrosis
Age (years)	55 [28;78]	54 [26;78]
Gender ratio (male:female)	6:6	6:6
Plasma creatinine (μmol L^{-1})	76.3 ± 10.7	105.8 ± 7.1*
Urea (mmol L^{-1})	4.1 ± 0.4	7.0 ± 0.8†
eGFR (ml min^{-1})	79.7 ± 4.0*	62.1 ± 7.2
Blood pressure (mmHg)	145.6 ± 6.5 / 81.8 ± 2.7	155.3 ± 8.8 / 86.2 ± 4.3

Note: Differences in age, gender, blood pressure, and markers of kidney function in patients with hydronephrosis vs. control subjects. Values for age are presented as mean with range, while values for creatinine, urea, eGFR, and blood pressure are presented as mean ± SEM, and marked with a symbol, when statistically significant.

*$p < 0.05$;

†$P < 0.01$.

medulla showed no change in TxB_2 tissue concentration (Figure 6H). PGE_2 tissue level did not show any significant differences in kidney cortex or outer medulla between groups (Figure 6J,I).

3 | DISCUSSION

The present study shows anti-fibrotic effects of COX-2 early at 7 days in the murine kidney fibrosis model of unilateral ureter obstruction. Within this[14] and other cohorts of mice[32] and rats,[8] UUO is associated with elevated COX-2 in kidneys. We now show that COX-2 mitigated early induction of extracellular matrix mRNAs and preserved angiogenic factor expression. In line, COX-2-deficient primary cultures of renal fibroblasts showed increased collagen mRNA. COX-2 deletion was associated with lower level of angiogenic factor mRNA levels and capillary rarefaction obstruction. This was not confirmed at protein level for VEGF. This could be due to delayed responsiveness at protein level or be due to antibody reactivity toward only some VEGF isoforms. In a series of human kidneys from patients with hydronephrosis there was significant interstitial fibrosis. While COX-1, COX-2, PTGE-S, and PGI-S enzymes, IP and TP receptor mRNAs in kidneys had a similar abundance between patient-groups, there was an increased EP_2 receptor abundance and increased thromboxane pathway (TxAS and TxB_2). Although patients discontinue medication 2 days before nephrectomy, some carry-over effects cannot be excluded. Some administered drugs are known to stimulate COX-2 (ACEi, AT1 blockers, diuretics) while others (e.g., NSAIDs and aspirin) exert variable inhibition of COX-1/-2 enzyme activity. Despite the overweight of COX-2 stimulating drugs in the hydronephrosis group, there was no upregulation of COX-2. The elevated thromboxane abundance in the hydronephrosis group is likely underestimated because some patients (3 out of 12) ingested NSAIDs.

The study reveals similarities (EP_2 receptor upregulation) and differences (COX-2 and EP_4 receptor level) between mouse and human kidney with obstruction and fibrosis. This may reflect both temporal aspects (acute vs. chronic), severity (complete vs. partial ureter occlusion), and species differences (mouse vs. human). Of translational importance, COX-products are substrates for preferential conversion by the thromboxane pathway in both cortex and medulla in chronic fibrosis in human kidney, while a similar level of PGE_2 as in control may signal preferentially through upregulated, protective, EP_2 receptor. This observation on one hand underlines the difficulty in predicting long term responses to COX-inhibitor treatment in clinical settings, which is confounded also by effects on GFR and perfusion, and, on the other hand, suggests that targeting specific pathways downstream of COX (Tx synthase, EP_2 receptors) would allow for more specific therapeutic effects.

3.1 | Antifibrotic effects of COX-2

Deletion of COX-2, but not COX-1, leads to mild kidney injury, fibrosis, and hypertension with age most pronounced in male mice at 129/Sv background.[36–41] This tendency is further aggravated after 7 days UUO in COX-2 KO mice with accumulation of collagens, both early fibrotic phase collagen type III,[42] and established phase fibrosis collagen I.[43] Sham-operated COX-2 deficient mice on the C57BL/6J genetic background of this study showed a mild renal phenotype at the age of 10–14 weeks, with no apparent histological difference between wild-type littermates (confirmed by morphological assessment). The influence of genetic background for the severity of renal phenotype has previously been documented.[40] Mice with

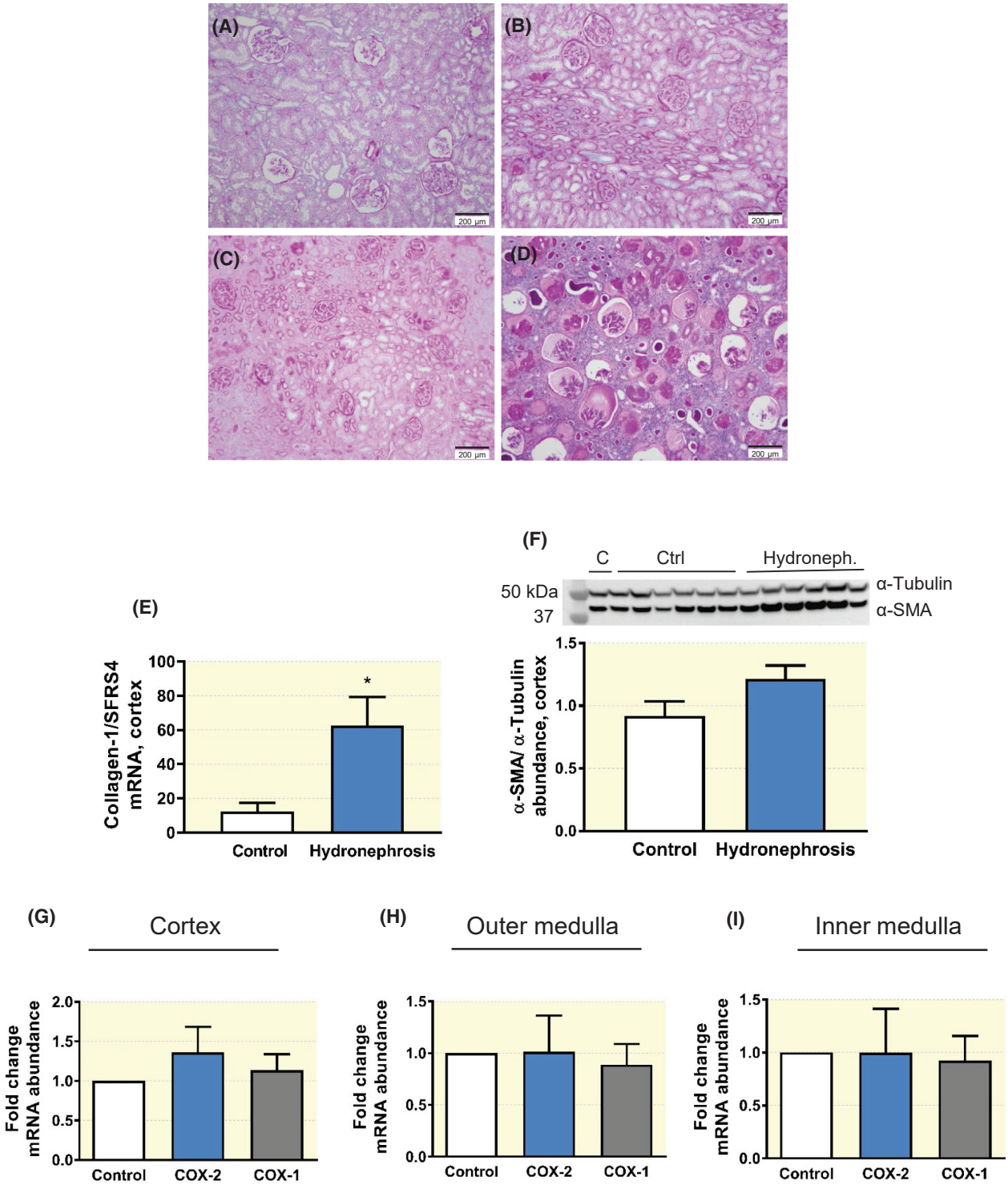

FIGURE 4 Fibrosis and COX enzyme abundance in patients with hydronephrosis and age- and gender-matched patients without hydronephrosis (control). Kidney sections from patients ($n = 12$) with hydronephrosis were stained by periodic acid-Schiff (PAS). Expansion of extracellular matrix, sclerotic glomeruli, and thickened basal lamina material (pink color) is associated with degree of fibrosis (A–D). Interstitial fibrosis (IF) score was determined according to Sethi et al.[35] Representative kidney slices with IF score 0 (A), 1 (B), 2 (C), and 3 (D) are shown. Scale bar in right corner corresponds to 200 µm. (E) shows abundance of collagen-1 mRNA, and diagram (F) shows immunoblotting for alpha-smooth actin (α-SMA) protein in kidney cortex tissue from patients with ($n = 12$) and without ($n = 12$) hydronephrosis. Diagram (G–I) shows kidney tissue abundance of COX-2 and COX-1 mRNAs in cortex (G), outer medulla (H), and inner medulla (I) in patients with hydronephrosis ($n = 12$) and control subjects ($n = 12$). Results are expressed as fold change in hydronephrotic patients compared to controls. (*) $p < 0.05$.

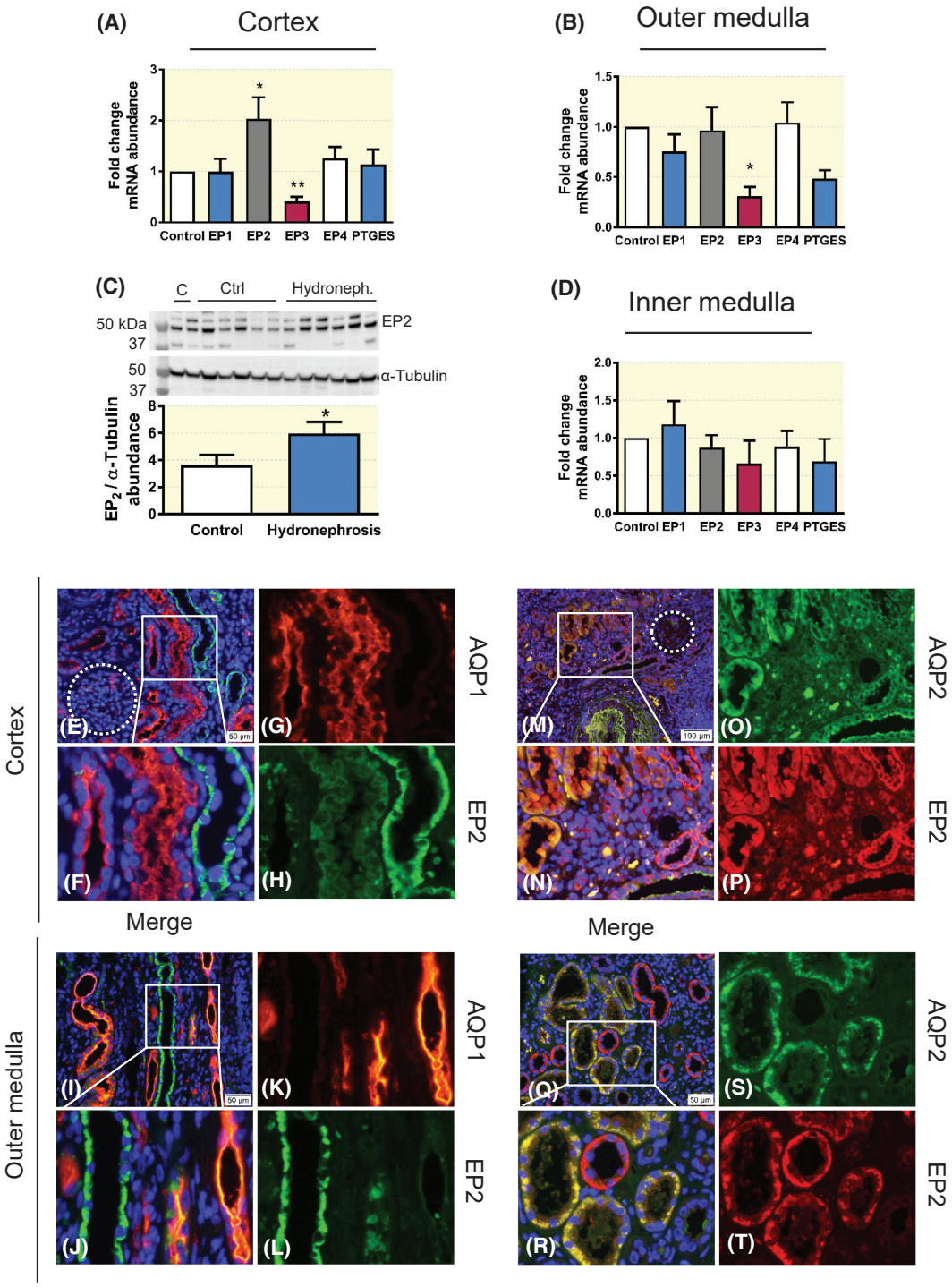

FIGURE 5 Kidney tissue abundance of PGE_2-EP receptors and PGE_2-synthase in patients with hydronephrosis and fibrosis and age- and gender-matched controls. Abundance of PGE_2-$EP_{1\text{-}4}$ receptors and PGE_2 synthase (PTGES) mRNAs in cortex (A), outer medulla (B), and inner medulla (C) in patients with hydronephrosis ($n = 12$) and control subjects ($n = 12$). Results shown in diagrams (A–C) are expressed as fold change in patients with hydronephrosis compared to controls. (D) shows immunoblotting data from cortex tissue homogenate from patients with hydronephrosis and control for PGE_2-EP_2 receptor (D, 52 kDa). Double fluorescent immunolabeling of tissue sections from hydronephrosis group for AQP1 and EP_2 receptor (E–L) and AQP2 and EP_2 receptor (M–T). Labeled segments for EP_2 co-localized with AQP2 (M–T) but not AQP1 (E–L). (*) $p < 0.05$, (†) $p < 0.01$.

C57BL/6J background developed a mild renal phenotype compared to 129/C57 mice from the original breeder pairs.[36] The possibility that COX-2 deficient mice are more prone to developing kidney fibrosis after UUO due to congenital renal defects cannot be eliminated. A pharmacological study using a selective COX-2 inhibitor in the

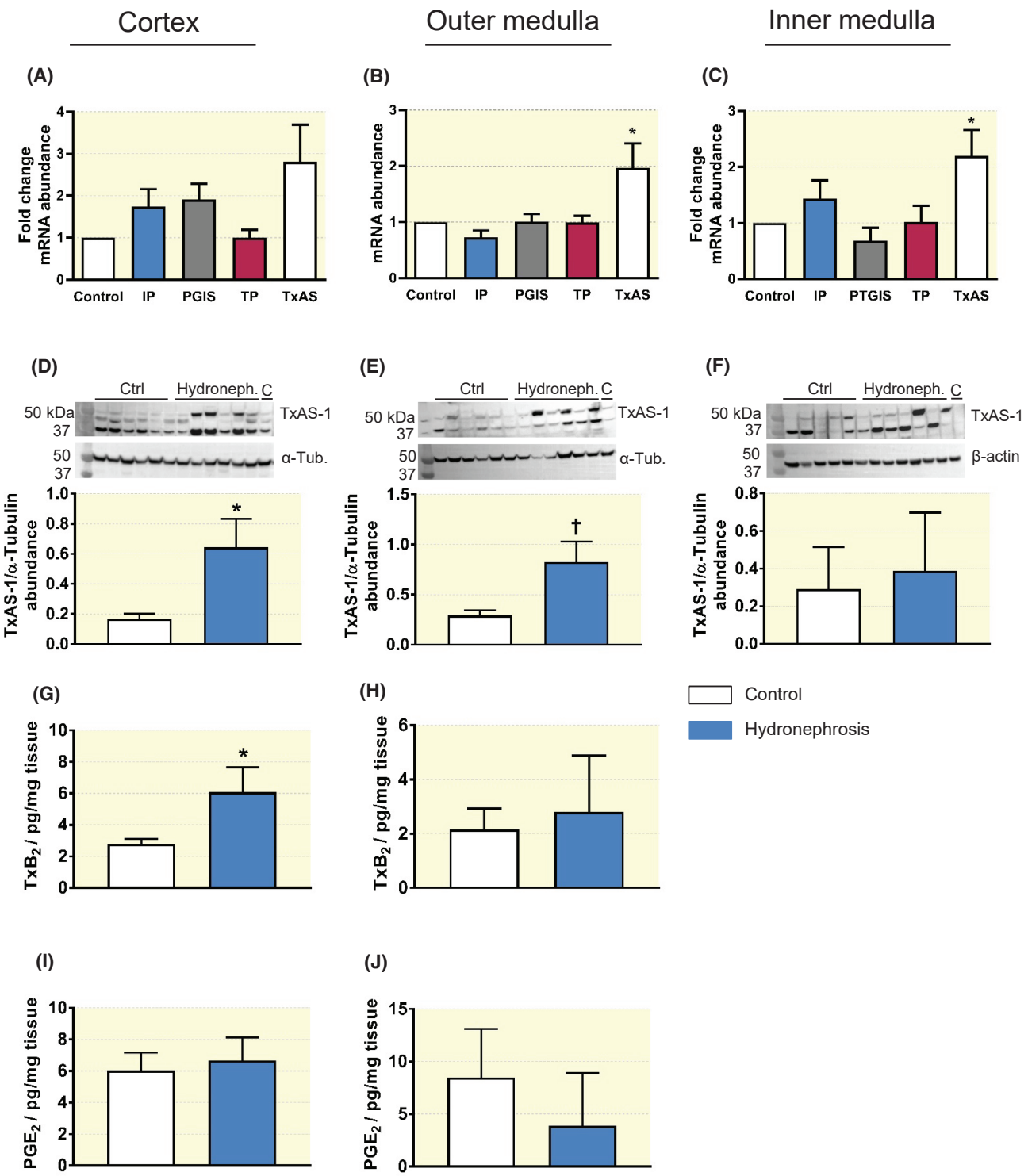

FIGURE 6 Kidney tissue prostanoid profiling in patients with hydronephrosis and fibrosis and control subjects. All data are from kidney tissue (cortex, outer, and inner medulla) homogenates from patients subjected to unilateral nephrectomy due to hydronephrosis ("Hydroneph", $n = 12$) and from subjects nephrectomized due to cancer ("control" $n = 12$). Kidney tissue mRNA abundance was determined by qPCR for prostacyclin receptor (IP), prostacyclin synthase (PGIS), thromboxane prostanoid (TP) receptor, and thromboxane synthase (TxAS) in cortex (A), outer medulla (B), and inner medulla (C). Protein levels were assessed by immunoblotting for TxAS-1 in cortex (D), outer (E), and inner medulla (F, 60 kDa). Tissue level of prostanoids TxB_2 and PGE_2 was determined by mass spectrometry in kidney cortex (G, I) and outer medulla fractions (H, J). (*) $p < 0.05$, (†) $p < 0.01$.

model of UUO corroborates the present data and found an increased interstitial ECM deposition in celecoxib-treated UUO mice compared to vehicle.[6] Uncertainties with the use of a pharmacological model are related to dose and pharmacokinetic differences, drug susceptibility between sexes, toxicology, and animal stress by drug administration. UUO increases COX-2 and mPGES.[10,44,45] Thus, COX-2 exerts anti-fibrotic action at least after 7 days,[6] an effect found also in lung.[28,46] We confirm that COX-2 is localized in interstitial fibroblasts after obstruction of murine kidney[10] with the strongest signal from the medulla where the fold-change in COX-2 abundance is largest.[10] COX-2 is important for the survival of renal interstitial cells after osmotic stress and mechanical stretch.[47–49] Cultured fibroblasts from COX-2 KO mice confirmed dysregulated synthesis and amplified mRNA abundance of ECM protein. Wild-type fibroblasts subjected to non-selective indomethacin did not recapitulate this, suggesting either insufficient COX-2 inhibition, an effect dissociated from COX-2 activity or related to environmental differences in vitro vs. in vivo. Furthermore, cell sorting was not conducted, and it cannot be ruled out that cells have differentiated in different directions during ontogeny. Also, serum starvation of cells prior to experiments likely attenuated COX-2 abundance and masked potential effects.

The UUO-induced COX-2 increase is highly transient in obstructed rat kidney.[50] Pharmacological interventions showed that COX-2 accounts predominantly for the transient accumulation of PGE_2 in cortex/outer medulla of obstructed rat kidney.[10] The absence of change in COX-2 (or COX-1), PGE-S and tissue PGE_2 concentration in human kidney with chronic obstruction corroborates the observation from rat kidney that the PGE_2 signal is transient. On the other hand, existing data show increased COX-2 mRNA abundance in end-stage human kidneys removed surgically after significant artery stenosis and ischemia,[51] a condition not comparable to the kidneys in the present study. COX-2 is increased in human ureter wall with obstruction, but kidney parenchyma was not previously investigated.[50,52] It is concluded that the PGE_2 synthesis pathway is not altered in the more chronic fibrotic setting of ureter obstruction.

At a molar level, PGE_2 is the major prostanoid accumulated in kidney tissue after UUO in chronic kidney disease.[10,34] Although PGE_2 is present in fibrotic human kidney tissue in similar levels as in non-fibrotic tissue, a shift in PGE_2-EP receptor subtype expression pattern may favor an anti-fibrotic action of PGE_2. The EP_2 receptor was upregulated in the fibrotic human kidney tissue as in murine kidney[14,32] and downregulation of EP_3 was confirmed in human kidney as observed in murine kidney.[14] Significant downregulation of PGE_2-signaling through EP_3 is a consistent finding in pro-fibrotic models which could also contribute to downstream beneficial effects of increased COX-2, a notion that was not tested. An EP_2 receptor agonist butaprost protects against fibrosis in vivo and in human kidney slices ex vivo.[53,54] EP_2 receptor is an attractive target to counter fibrosis in chronic kidney disease in humans whereas in mice, PGE_2 may also act through EP_4 receptors which are upregulated.[32] Such upregulation was not seen in fibrotic human kidney. We have previously shown that increased COX-2 protects against apoptosis and oxidative stress following UUO.[14] The association of EP_2 receptors with epithelial cells in outer medulla tubular segments that experience ischemia and osmotic stress but which do not participate in regulated water transport would be compatible with cAMP-mediated survival effects described both in renal[55] but also intestinal epithelia.[56]

Myofibroblasts are responsible for the exaggerated ECM synthesis and secretion during fibrosis (reviewed in Ref. [57]) and in mouse kidneys with obstruction, COX-2 was associated with myofibroblasts. There was a significant accumulation of α-SMA–positive interstitial cells and enhanced α-SMA abundance in COX-2 KO UUO mice suggesting that COX-2 normally attenuates myofibroblast activity, an effect mimicked in mice by EP_4 receptor agonist[32,34] but also PGE_2-EP_2 receptor agonist.[27]

Cortex and outer medulla regions of human hydronephrotic kidneys showed increased thromboxane synthase protein abundance confirmed by increased cortex tissue concentration of TxB_2. In agreement, TxB_2 was increased in tissue from obstructed rat kidney.[10] Treatment with a TxAS inhibitor decreased TxB_2 and improved urine output and clearance in hydronephrotic rat.[58] Cortical microsomes from human hydronephrotic kidneys showed TxB_2 as the major metabolite and inhibition of TxAS ex vivo reduced TXB_2 production.[59] In the 5/6 nephrectomy injury model in rats, treatment with a TxA_2 receptor antagonist and the synthesis inhibitor ridogrel had beneficial effect on hypertension and increased kidney function.[60] The sum of data converge by showing significant beneficial effects not only on fibrosis but also kidney function by targeting TxAS and TxB_2 in chronic kidney disease settings.

3.2 | Summary and conclusion

In a murine model of UUO-induced fibrosis, COX-2 was upregulated in interstitial fibroblasts in kidney. Deletion of COX-2 promoted fibrosis, enhanced myofibroblast expansion and extracellular matrix deposition, including collagen I and III accumulation. Human kidneys from patients with ureter obstruction and hydronephrosis showed fibrosis but no change in COX-1, COX-2, PTGES, PGI-S, IP, TP, EP_1, and EP_4 mRNAs in cortex and medulla. Obstructed human and murine kidneys responded similarly with upregulation of PGE_2-EP_2 and downregulation

of EP_3 receptor. Kidneys from hydronephrotic patients exhibited increased TxAS and TxB_2 tissue concentration. We conclude that the absence of COX-2 activity in mice promotes kidney fibrosis and thus that COX-2 activity is likely to mitigate fibrosis and preserves microvasculature up to 7 days after an ~~in~~ injury. Downstream of COX-2, thromboxane synthase, EP_2 receptor, and TP receptor are potential pharmacological targets to counter interstitial fibrosis in human chronic kidney disease.

4 | METHODS

4.1 | Human kidney tissue

Human kidney tissue samples were obtained from patients undergoing unilateral nephrectomy at the Department of Urology, Odense University Hospital. Nephrectomy was performed due to, for example, recurring infection or resistant hypertension after confirmed hydronephrosis of loss of functional contribution by scintigraphy. Tissue samples were collected from patients only with a pathologically verified diagnosis of hydronephrosis ($n = 12$). Normally appearing kidney tissue from age- and gender-matched patients undergoing nephrectomy due to kidney cancer was used as control subjects ($n = 12$). Tissue samples were removed and either snap-frozen in liquid nitrogen or fixed in 4% paraformaldehyde (PFA) within approximately 60 min of removal from the patient. Tissue was embedded in paraffin or stored at −80°C until used for analyses. The study was approved by the Regional Committees on Health Research Ethics for Southern Denmark (S-20140159) and the Danish Data Protection Agency (18/1107). All patients gave written informed consent before inclusion in the study.

4.2 | Animals

Animal experiments conformed to the guidelines for care and use of laboratory animals (NIH Publication No. 85-23, Revised 1996) and approvals as described previously.[14] Procedures for backcrossing of COX-2 KO mice and wild-type littermate controls to the C57BL/6J genetic background,[14] genotyping,[61] and housing of animals[14] were performed as previously described. Breeding was done at the Biomedical Laboratory, University of Southern Denmark.

4.3 | Experimental design and surgical procedures

UUO was induced for 7 days in COX-2 KO mice and WT littermates. Age- and time-matched sham-operated controls were prepared and observed in parallel with each experimental group. Both male and female mice were represented in each experimental group, in an approximately 1:1 ratio (gender distribution between groups available in Table 1). The surgical procedures, harvesting of blood and kidneys were performed as described previously.[14] Kidney tissue fractions (cortex-outer medulla) used for RNA (WT sham: $n = 17$, COX-2 KO sham: $n = 12$, WT 7dUUO: $n = 17$, and COX-2 KO 7dUUO: $n = 11$) and protein analysis ($n = 6$ in each group) as well as kidneys from animals fixed by systemic perfusion with PFA (WT sham: $n = 5$, COX-2 KO sham: $n = 3$, WT 7dUUO: $n = 4$, and COX-2 KO 7dUUO: $n = 3$) were harvested from mice used in previous publication.[14] Plasma creatinine, sodium (Na^+), urea, and potassium (K^+) were measured using Roche Cobas 6000 Analyzer (Roche Diagnostic, Basel, Switzerland). Plasma osmolality was measured using freezing-point depression (Osmomat 030-D, Gonotec, Berlin, Germany) (Table 1).

4.4 | mRNA analyses

Total RNA was extracted using the RNeasy Protect Mini Kit (Qiagen) and eluted in RNase-/DNase-free water. RNA concentration was quantified by spectrophotometry (NanoPhotometer, Implem; AH Diagnostics). Complementary DNA synthesis, PCR analyses, and quantitative PCR experiments were performed as described previously.[62] For quantitative PCR analyses, a standard curve was constructed by plotting threshold cycle (C_t values) against serial dilutions of purified PCR product. Specificity was confirmed by post-run melting point analyses and gel electrophoresis. Primer sequences are available in Table S3 or as previously published.[63]

4.5 | Western blotting

Tissue samples were homogenized in a sucrose/imidazole buffer as described previously.[62] Protein concentration was determined using the Quick Start Bradford Protein Assay (Biorad) using a serial dilution of BSA as standard. For western blotting, 10–30 μg of protein was separated by SDS-PAGE in a 4%–12% Bis-Tris gel (Invitrogen). By use of the XCell SureLock Mini-Cell System (Invitrogen), proteins were transferred to an activated 0.45 μm pore-size polyvinylidene difluoride membrane (Immobilon-P Transfer Membrane; Millipore). Membranes were blocked with 5% non-fat dry milk in TBST (137 mM NaCl, 20 mM Tris at pH 7.6, 0.05% Tween 20) before incubation with primary antibodies. The antigen–antibody complex was

visualized by horseradish peroxidase-conjugated secondary antibodies (P0448, P0447, 1:2000; DAKO) using the enhanced chemiluminescence system (Amersham Pharmacia Biotech or PerkinElmer). Primary antibodies were COX-1 (160 109, 1:1000; Cayman Chemicals), GAPDH (ab9585, 1:10 000; Abcam), α-smooth muscle actin (α-SMA) (ab5694, 1:10 000, Abcam), VEGF (ab46154, 1:10 000, Abcam), EP_2 (101 750, 1:1000; Cayman Chemicals), and β-tubulin (ABT171, 1:10 000; Sigma-Aldrich). Non-cropped images of membranes are available in supplement.

4.6 | Total collagen analysis

Total collagen abundance in kidney cortex-outer medulla tissue fractions from sham and UUO mice was assessed by hydroxyproline content. Assay procedure was performed according to the manufacture's instructions (Total Collagen Assay Kit, ab222942, Abcam). In brief, tissue samples were homogenized in RNase-free water (Gibco) and boiled in 10 N NaOH at 120°C for 2 h. A commercial positive collagen control was run in parallel. Samples were analyzed on a VersaMax ELISA microplate reader (Molecular Devices, California, USA).

4.7 | Prostanoid analysis by LC–MS/MS

Prostanoids were extracted from 5 to 10 mg homogenized whole renal tissue samples, and abundances were measured by LC–MS/MS as described previously.[62] In short, renal tissue samples were incubated with the extraction buffer containing 600 μl ethyl acetate, 100 μl 0.15 M ethylenediamine tetraacetic acid solution, and 20 μl internal standard solution. Samples were homogenized using a Mixer Mill MM400 (Retsch, Haan, Germany) and zirconium oxide grinding balls (diameter 3 mm). Following centrifugation at 20 000 *g* for 5 min, the organic phase was collected. The extraction was repeated, and the pooled organic phases were removed at 45°C under nitrogen. For reconstitution, 50 μl water/acetonitrile 8:2 (v/v) with 0.0025% formic acid was used and injected (10 μl) into the LC–MS/MS system. PBS was used as surrogate matrix for the preparation of calibration standards (Cayman Chemical, Ann Arbor, MI, USA) and quality control samples. Prostanoids were separated with a Synergi Hydro RP HPLC column 2.0 × 150 mm and Pre-Column 2.0 × 2 mm (Phenomenex, Waldbronn, Germany). A gradient elution using water and acetonitrile with 0.0025% formic acid was applied. Analyst Software 1.6.3 and MultiQuant Software 3.0.2 (both Sciex, Darmstadt, Germany) was used for data acquisition and quantification. Calibration curves were calculated by linear regression with $1/x^2$ weighting.

4.8 | Renal morphology

Renal morphology was evaluated in periodic acid-Schiff (PAS) stained kidney sections. For the human cohort, interstitial fibrosis was scored according to Sethi et al.[35] In an observer-blinded design, the percentage of the cortical region affected by interstitial fibrosis was scored according to the following: 0: <10%, 1: 10%–25%, 2: 26%–50%, and 3: >50%.

4.9 | Histochemistry

Tissue sections were deparaffinized with Tissue Tec-Tissue Clear (Sakura PsoHosp) and rehydrated in graded ethanol series (99.9%–70%). Antigen retrieval was performed by boiling in a microwave for 20 min., in a pressure cooker for 5 min. or in a heating cabinet at 60°C for 16 h. Buffers were either TEG (10 mM Tris, 0.5 mM EGTA, pH 9.0), TRS (Dako), or citrate buffer (Dako). Primary antibodies used were as follows: Collagen I (ab34710, 1:250, Abcam), Collagen III (ab7778, 1:50, Abcam), α-SMA (ab5694, 1:2000, Abcam), CD34 (ab8158, 1:1000, Abcam), and EP_2 (101 750, 1:1000, Cayman Chemicals). CD34 was visualized using the Envision+ System (K4002, Dako). A negative control with omission of primary antibody was run in parallel.

Collagen I positive area was determined in kidney tissue slides by point counting using the VIS image analysis tool (Visiopharm). Analyses were done at 4× magnification with the observer blinded to the experimental groups.

Double fluorescence labeling of tissue sections was performed by use of TSA Cyanine 3 detection kit (#SAT704A001EA, Akoya Biosciences, USA). In brief, after deparaffinization and antigen retrieval, endogen peroxidase activity was blocked by incubation of sections with 1.5% H_2O_2/TBST. Next, slides were incubated with the first primary antibody and the secondary antibody, followed by incubation with cyanine-3 tyramide reagent (in dark chamber). In the following steps, slides were shed from light. Antigen retrieval was repeated followed by incubation with the second primary antibody and fluorescent secondary antibody (Alexa fluor 488, #A11034, 1:500, Thermo Scientific). Nuclei were labeled with 0.1 $\mu g\,ml^{-1}$ DAPI (D9542, 1:1000, Sigma Aldrich) and sections mounted with fluorescence mounting medium (Merck). Primary antibodies used for double fluorescent labeling were as follows: EP_2 (101 750, 1:1000, Cayman Chemicals),

AQP1 (ab15080, 1:500, Abcam), and AQP2 (sc-9882, 1:200, Santa Cruz).

4.10 | Cell cultures

Primary cultures of renal fibroblasts were isolated as described previously.[64] In short, both kidneys were removed from 1 WT and 1 COX-2 KO mouse and placed in sterile PBS, pH 7.4 on ice. Kidneys were minced in a petri dish using a razor blade and then transferred to T75 cell culture flasks with RPMI (Gibco) supplemented with 10% fetal calf serum (Gibco) and 1% penicillin/streptomycin solution (Gibco). Cells were cultured through four to five generations before being used for experiments. Twenty hours before initiation of experiments, serum-free medium (SFM) was added to the cells (RPMI supplemented with 0.5% bovine serum albumin (Gibco) and 1% penicillin/streptomycin solution (Gibco)). For experiments, cells were either harvested at baseline (WT and COX-2 KO fibroblasts) or stimulated with indomethacin (10 μM, Sigma Aldrich), NS-398 (10 μM, Sigma Aldrich), (Valeryl Salicylate, 500 μM, Sigma Aldrich), or vehicle (DMSO 0.1%) for 24 h. Cells were lysed with RLT buffer from the RNeasy Protect Mini Kit (Qiagen) supplemented with β-mercaptoethanol (10 $\mu l\, ml^{-1}$) and snap-frozen in liquid nitrogen. Samples were stored at −80°C before use.

4.11 | Statistics

A one-way analysis of variance (ANOVA) with Bonferroni's comparisons test was used to determine significant differences between groups of the experimental animal series. Unpaired Student's *t*-test was used to analyze data from the human hydronephrotic cohort. For non-Gaussian distributed data, Mann–Whitney test or Kruskal Wallis with Dunn's post hoc test was used. p Values <0.05 were considered statistically significant. Values are presented as means ± SEM for Gaussian distributed and median with IQR for non-Gaussian distributed data. GraphPad Prism software (version 7.0) was applied for data analysis.

ACKNOWLEDGMENTS

The authors thank Kristoffer Rosenstand and Inger Nissen as well as Gitte Skou and Gitte Kall for expert technical assistance.

FUNDING INFORMATION

This work was supported by the following foundations and institutions: Odense University Hospital PhD Fund, University of Southern Denmark, Hede Nielsen Foundation, Aase, and Ejnar Danielsen Foundation, The A.P. Møller Foundation for the Advancement of Medical Science, Helen, and Ejnar Bjørnow Fund, Danish Society of Nephrology, and Danish Kidney Association as well as by Danish Council for Independent Research, grant no. 6110-00231B, Aarhus University Research Foundation, grant no. AUFF-E-2015-FLS-8-69 (received by R.N.).

CONFLICT OF INTEREST

The authors have no conflict of interest to declare.

DATA AVAILABILITY STATEMENT

Data will be available on request from a third party. Because of the sensitive nature of the data collected from patients, reasonable requests to access the dataset from qualified researchers trained in human subject confidentiality protocols may be sent to the corresponding author.

ORCID

Signe S. Tofteng https://orcid.org/0000-0002-5400-4272
Rikke Nørregaard https://orcid.org/0000-0002-0580-373X
Claus Bistrup https://orcid.org/0000-0002-9280-916X
Boye L. Jensen https://orcid.org/0000-0001-7607-213X
Kirsten Madsen https://orcid.org/0000-0002-1427-602X

REFERENCES

1. Bohle A, Christ H, Grund KE, Mackensen S. The role of the interstitium of the renal cortex in renal disease. *Contrib Nephrol*. 1979;16:109-114.
2. Møller JC, Skriver E, Olsen S, Maunsbach AB. Ultrastructural analysis of human proximal tubules and cortical interstitium in chronic renal disease (hydronephrosis). *Virchows Arch A Pathol Anat Histopathol*. 1984;402(3):209-237.
3. Nadasdy T, Laszik Z, Blick KE, Johnson DL, Silva FG. Tubular atrophy in the end-stage kidney: a lectin and immunohistochemical study. *Hum Pathol*. 1994;25(1):22-28.
4. Zeisberg M, Neilson EG. Mechanisms of tubulointerstitial fibrosis. *J Am Soc Nephrol*. 2010;21(11):1819-1834.
5. Harris RC, McKanna JA, Akai Y, Jacobson HR, Dubois RN, Breyer MD. Cyclooxygenase-2 is associated with the macula densa of rat kidney and increases with salt restriction. *J Clin Invest*. 1994;94(6):2504-2510.
6. Kamata M, Hosono K, Fujita T, Kamata K, Majima M. Role of cyclooxygenase-2 in the development of interstitial fibrosis in kidneys following unilateral ureteral obstruction in mice. *Biomed Pharmacother*. 2015;70:174-180.
7. Cheng X, Zhang H, Lee HL, Park JM. Cyclooxygenase-2 inhibitor preserves medullary aquaporin-2 expression and prevents polyuria after ureteral obstruction. *J Urol*. 2004;172(6 Pt 1):2387-2390.
8. Chou SY, Cai H, Pai D, Mansour M, Huynh P. Regional expression of cyclooxygenase isoforms in the rat kidney in complete unilateral ureteral obstruction. *J Urol*. 2003;170(4 Pt 1):1403-1408.
9. Bonvalet JP, Pradelles P, Farman N. Segmental synthesis and actions of prostaglandins along the nephron. *Am J Physiol*. 1987;253(3 Pt 2):F377-F387.

10. Norregaard R, Jensen BL, Topcu SO, et al. Urinary tract obstruction induces transient accumulation of COX-2-derived prostanoids in kidney tissue. *Am J Physiol Regul Integr Comp Physiol*. 2010;298(4):R1017-R1025.
11. Nilsson L, Madsen K, Topcu SO, Jensen BL, Frøkiær J, Nørregaard R. Disruption of cyclooxygenase-2 prevents downregulation of cortical AQP2 and AQP3 in response to bilateral ureteral obstruction in the mouse. *Am J Physiol Renal Physiol*. 2012;302(11):F1430-F1439.
12. Norregaard R, Jensen BL, Li C, et al. COX-2 inhibition prevents downregulation of key renal water and sodium transport proteins in response to bilateral ureteral obstruction. *Am J Physiol Renal Physiol*. 2005;289(2):F322-F333.
13. Norregaard R, Jensen BL, Topcu SO, et al. COX-2 activity transiently contributes to increased water and NaCl excretion in the polyuric phase after release of ureteral obstruction. *Am J Physiol Renal Physiol*. 2007;292(5):F1322-F1333.
14. Nilsson L, Madsen K, Krag S, Frøkiær J, Jensen BL, Nørregaard R. Disruption of cyclooxygenase type 2 exacerbates apoptosis and renal damage during obstructive nephropathy. *Am J Physiol Renal Physiol*. 2015;309(12):F1035-F1048.
15. Cheng H, Zhang M, Moeckel GW, et al. Expression of mediators of renal injury in the remnant kidney of ROP mice is attenuated by cyclooxygenase-2 inhibition. *Nephron Exp Nephrol*. 2005;101(3):e75-e85.
16. Wang X, Yao B, Wang Y, et al. Macrophage Cyclooxygenase-2 protects against development of diabetic nephropathy. *Diabetes*. 2017;66(2):494-504.
17. Wang JL, Cheng HF, Shappell S, Harris RC. A selective cyclooxygenase-2 inhibitor decreases proteinuria and retards progressive renal injury in rats. *Kidney Int*. 2000;57(6):2334-2342.
18. Jo YI, Cheng H, Wang S, Moeckel GW, Harris RC. Puromycin induces reversible proteinuric injury in transgenic mice expressing cyclooxygenase-2 in podocytes. *Nephron Exp Nephrol*. 2007;107(3):e87-e94.
19. Yang C, Nilsson L, Cheema MU, et al. Chitosan/siRNA nanoparticles targeting cyclooxygenase type 2 attenuate unilateral ureteral obstruction-induced kidney injury in mice. *Theranostics*. 2015;5(2):110-123.
20. Hsu CC, Wang H, Hsu YH, et al. Use of nonsteroidal anti-inflammatory drugs and risk of chronic kidney disease in subjects with hypertension: Nationwide longitudinal cohort study. *Hypertension*. 2015;66(3):524-533.
21. Gooch K, Culleton BF, Manns BJ, et al. NSAID use and progression of chronic kidney disease. *Am J Med*. 2007;120(3):280.e1-280.e7.
22. Dackor RT, Cheng J, Voltz JW, et al. Prostaglandin E(2) protects murine lungs from bleomycin-induced pulmonary fibrosis and lung dysfunction. *Am J Physiol Lung Cell Mol Physiol*. 2011;301(5):L645-L655.
23. Elias JA, Rossman MD, Zurier RB, Daniele RP. Human alveolar macrophage inhibition of lung fibroblast growth. A prostaglandin-dependent process. *Am Rev Respir Dis*. 1985;131(1):94-99.
24. Fine A, Poliks CF, Donahue LP, Smith BD, Goldstein RH. The differential effect of prostaglandin E2 on transforming growth factor-beta and insulin-induced collagen formation in lung fibroblasts. *J Biol Chem*. 1989;264(29):16988-16991.
25. Huang S, Wettlaufer SH, Hogaboam C, Aronoff DM, Peters-Golden M. Prostaglandin E(2) inhibits collagen expression and proliferation in patient-derived normal lung fibroblasts via E prostanoid 2 receptor and cAMP signaling. *Am J Physiol Lung Cell Mol Physiol*. 2007;292(2):L405-L413.
26. Kohyama T, Ertl RF, Valenti V, et al. Prostaglandin E(2) inhibits fibroblast chemotaxis. *Am J Physiol Lung Cell Mol Physiol*. 2001;281(5):L1257-L1263.
27. Kolodsick JE, Peters-Golden M, Larios J, Toews GB, Thannickal VJ, Moore BB. Prostaglandin E2 inhibits fibroblast to myofibroblast transition via E. prostanoid receptor 2 signaling and cyclic adenosine monophosphate elevation. *Am J Respir Cell Mol Biol*. 2003;29(5):537-544.
28. Lama V, Moore BB, Christensen P, Toews GB, Peters-Golden M. Prostaglandin E2 synthesis and suppression of fibroblast proliferation by alveolar epithelial cells is cyclooxygenase-2-dependent. *Am J Respir Cell Mol Biol*. 2002;27(6):752-758.
29. Hui AY, Dannenberg AJ, Sung JJY, et al. Prostaglandin E2 inhibits transforming growth factor beta 1-mediated induction of collagen alpha 1(I) in hepatic stellate cells. *J Hepatol*. 2004;41(2):251-258.
30. Koide S, Kobayashi Y, Oki Y, Nakamura H. Prostaglandin E2 inhibits platelet-derived growth factor-stimulated cell proliferation through a prostaglandin E receptor EP2 subtype in rat hepatic stellate cells. *Dig Dis Sci*. 2004;49(9):1394-1400.
31. Rieder F, Georgieva M, Schirbel A, et al. Prostaglandin E2 inhibits migration of colonic lamina propria fibroblasts. *Inflamm Bowel Dis*. 2010;16(9):1505-1513.
32. Nakagawa N, Yuhki KI, Kawabe JI, et al. The intrinsic prostaglandin E2-EP4 system of the renal tubular epithelium limits the development of tubulointerstitial fibrosis in mice. *Kidney Int*. 2012;82(2):158-171.
33. Vukicevic S, Simic P, Borovecki F, et al. Role of EP2 and EP4 receptor-selective agonists of prostaglandin E(2) in acute and chronic kidney failure. *Kidney Int*. 2006;70(6):1099-1106.
34. Luo R, Kakizoe Y, Wang F, et al. Deficiency of mPGES-1 exacerbates renal fibrosis and inflammation in mice with unilateral ureteral obstruction. *Am J Physiol Renal Physiol*. 2017;312(1):F121-F133.
35. Sethi S, D'Agati VD, Nast CC, et al. A proposal for standardized grading of chronic changes in native kidney biopsy specimens. *Kidney Int*. 2017;91(4):787-789.
36. Dinchuk JE, Car BD, Focht RJ, et al. Renal abnormalities and an altered inflammatory response in mice lacking cyclooxygenase II. *Nature*. 1995;378(6555):406-409.
37. Khan KN, Stanfield KM, Dannenberg A, et al. Cyclooxygenase-2 expression in the developing human kidney. *Pediatr Dev Pathol*. 2001;4(5):461-466.
38. Komhoff M, Wang JL, Cheng HF, et al. Cyclooxygenase-2-selective inhibitors impair glomerulogenesis and renal cortical development. *Kidney Int*. 2000;57(2):414-422.
39. Morham SG, Langenbach R, Loftin CD, et al. Prostaglandin synthase 2 gene disruption causes severe renal pathology in the mouse. *Cell*. 1995;83(3):473-482.
40. Yang T, Huang YG, Ye W, Hansen P, Schnermann JB, Briggs JP. Influence of genetic background and gender on hypertension and renal failure in COX-2-deficient mice. *Am J Physiol Renal Physiol*. 2005;288(6):F1125-F1132.
41. Zhang MZ, Wang JL, Cheng HF, Harris RC, McKanna JA. Cyclooxygenase-2 in rat nephron development. *Am J Physiol*. 1997;273(6 Pt 2):F994-F1002.

42. Clore JN, Cohen IK, Diegelmann RF. Quantitation of collagen types I and III during wound healing in rat skin. *Proc Soc Exp Biol Med*. 1979;161(3):337-340.
43. Trojanowska M, Carwile LeRoy E, Eckes B, Krieg T. Pathogenesis of fibrosis: type 1 collagen and the skin. *J Mol Med (Berl)*. 1998;76(3-4):266-274.
44. Carlsen I, Donohue KE, Jensen AM, et al. Increased cyclooxygenase-2 expression and prostaglandin E2 production in pressurized renal medullary interstitial cells. *Am J Physiol Regul Integr Comp Physiol*. 2010;299(3):R823-R831.
45. Park JM, Yang T, Arend LJ, et al. Obstruction stimulates COX-2 expression in bladder smooth muscle cells via increased mechanical stretch. *Am J Physiol*. 1999;276(1 Pt 2):F129-F136.
46. Lovgren AK, Jania LA, Hartney JM, et al. COX-2-derived prostacyclin protects against bleomycin-induced pulmonary fibrosis. *Am J Physiol Lung Cell Mol Physiol*. 2006;291(2):L144-L156.
47. Hao CM, Redha R, Morrow J, Breyer MD. Peroxisome proliferator-activated receptor delta activation promotes cell survival following hypertonic stress. *J Biol Chem*. 2002;277(24):21341-21345.
48. Rao R, Hao CM, Breyer MD. Hypertonic stress activates glycogen synthase kinase 3beta-mediated apoptosis of renal medullary interstitial cells, suppressing an NFkappaB-driven cyclooxygenase-2-dependent survival pathway. *J Biol Chem*. 2004;279(6):3949-3955.
49. Carlsen I, Frokiaer J, Norregaard R. Quercetin attenuates cyclooxygenase-2 expression in response to acute ureteral obstruction. *Am J Physiol Renal Physiol*. 2015;308(11):F1297-F1305.
50. Norregaard R, Jensen BL, Topcu SO, et al. Cyclooxygenase type 2 is increased in obstructed rat and human ureter and contributes to pelvic pressure increase after obstruction. *Kidney Int*. 2006;70(5):872-881.
51. Therland KL, Stubbe J, Thiesson HC, et al. Cycloxygenase-2 is expressed in vasculature of normal and ischemic adult human kidney and is colocalized with vascular prostaglandin E2 EP4 receptors. *J Am Soc Nephrol*. 2004;15(5):1189-1198.
52. Nakada SY, Jerde TJ, Jacobson LM, Saban R, Bjorling DE, Hullett DA. Cyclooxygenase-2 expression is up-regulated in obstructed human ureter. *J Urol*. 2002;168(3):1226-1229.
53. Guo NF, Qiu Z, Chen XL, Chen X, Huang JB, Liu J. Prostaglandin E2 receptor subtypes 1 and 2 play a role in TGF-beta1-induced renal fibrosis by regulating endoplasmic reticulum stress. *Eur Rev Med Pharmacol Sci*. 2020;24(9):4954-4962.
54. Jensen MS, Mutsaers HAM, Tingskov SJ, et al. Activation of the prostaglandin E2 EP2 receptor attenuates renal fibrosis in unilateral ureteral obstructed mice and human kidney slices. *Acta Physiol (Oxf)*. 2019;227(1):e13291.
55. Steinert D, Küper C, Bartels H, Beck FX, Neuhofer W. PGE2 potentiates tonicity-induced COX-2 expression in renal medullary cells in a positive feedback loop involving EP2-cAMP-PKA signaling. *Am J Physiol Cell Physiol*. 2009;296(1):C75-C87.
56. Nishihara H, Kizaka-Kondoh S, Insel PA, Eckmann L. Inhibition of apoptosis in normal and transformed intestinal epithelial cells by cAMP through induction of inhibitor of apoptosis protein (IAP)-2. *Proc Natl Acad Sci U S A*. 2003;100(15):8921-8926.
57. Barnes JL, Glass WF 2nd. Renal interstitial fibrosis: a critical evaluation of the origin of myofibroblasts. *Contrib Nephrol*. 2011;169:73-93.
58. Masumura H, Kunitada S, Irie K, Ashida S, Abe Y. A thromboxane A2 synthase inhibitor, DP-1904, prevents rat renal injury. *Eur J Pharmacol*. 1991;193(3):321-327.
59. Morrison AR, Thornton F, Blumberg A, Vaughan ED. Thromboxane A2 is the major arachidonic acid metabolite of human cortical hydronephrotic tissue. *Prostaglandins*. 1981;21(3):471-481.
60. Lariviere R, Moreau C, Rodrigue ME, Lebel M. Thromboxane blockade reduces blood pressure and progression of renal failure independent of endothelin-1 in uremic rats. *Prostaglandins Leukot Essent Fatty Acids*. 2004;71(2):103-109.
61. Friis UG, Madsen K, Svenningsen P, et al. Hypotonicity-induced renin exocytosis from juxtaglomerular cells requires aquaporin-1 and cyclooxygenase-2. *J Am Soc Nephrol*. 2009;20(10):2154-2161.
62. Staehr M, Hansen PB, Madsen K, Vanhoutte PM, Nüsing RM, Jensen BL. Deletion of cyclooxygenase-2 in the mouse increases arterial blood pressure with no impairment in renal NO production in response to chronic high salt intake. *Am J Physiol Regul Integr Comp Physiol*. 2013;304(10):R899-R907.
63. Madsen K, Marcussen N, Pedersen M, et al. Angiotensin II promotes development of the renal microcirculation through AT1 receptors. *J Am Soc Nephrol*. 2010;21(3):448-459.
64. Gooch JL, Roberts BR, Cobbs SL, Tumlin JA. Loss of the alpha-isoform of calcineurin is sufficient to induce nephrotoxicity and altered expression of transforming growth factor-beta. *Transplantation*. 2007;83(4):439-447.

SUPPORTING INFORMATION

Additional supporting information may be found in the online version of the article at the publisher's website.

How to cite this article: Tofteng SS, Nilsson L, Mogensen AK, et al. Increased COX-2 after ureter obstruction attenuates fibrosis and is associated with EP_2 receptor upregulation in mouse and human kidney. *Acta Physiol*. 2022;235:e13828. doi: 10.1111/apha.13828